Environmental Science and Pollution Research (2023) 30:35153–35169
https://doi.org/10.1007/s11356-022-24220-0

RESEARCH ARTICLE

Photocatalytic degradation of chlorazol yellow dye under sunlight irradiation using Ce, Bi, and N co-doped TiO_2 photocatalyst in neutral medium

Zannatul Mumtarin Moushumy[1] · **Mohammad Jobaer Hassan**[1] · **Mohebul Ahsan**[1] · **Md. Mahmudul Hasan**[2] · **Md. Nizam Uddin**[1] · **Yuki Nagao**[2] · **Mohammad A. Hasnat**[1]

Received: 15 July 2022 / Accepted: 10 November 2022 / Published online: 17 December 2022

Abstract

Chlorazol yellow (CY) is a commonly used anionic, toxic, mutagenic, and potentially carcinogenic azo dye, which is menacing to the environment, aquatic system, food chain, and human health as well. To remove CY dye molecules from an aqueous medium, a series of Ce, Bi, and N co-doped TiO_2 photocatalysts were prepared by varying the composition of the dopants. Under sunlight irradiation, the resultant 5 wt% (Ce-Bi-N) co-doped TiO_2 composite catalyst was found to show the best catalytic activity. Hence, the required characterization of this catalyst was performed systematically using energy-dispersive X-ray spectroscopy (EDX), scanning electron microscope (SEM), Fourier-transform infrared spectroscopy (FTIR), X-ray photoelectron spectroscopy (XPS), and X-ray diffraction (XRD) techniques. From the thorough investigation, it is revealed that the CY molecules reached adsorption–desorption equilibrium onto the surface of the catalyst within 30 min following second-order kinetics. Herein, the catalyst attained 97% degradation when exposed to sunlight at neutral (pH ~ 7, [CY] = 5 mg L^{-1}) medium. The developed catalyst can destruct CY molecules with a maximum rate of 23.1 μg CY g^{-1} min^{-1} and the photodegradation kinetics follows first-order kinetics below 23.5 mg L^{-1}, a fractional order between 23.5 and 35.0 mg L^{-1}, and a zeroth order above 35.0 mg L^{-1} of CY concentration. Finding from scavenging effect implies that O_2^- and $OH^\bullet$ radicals have significant influence on the degradation. A suitable mechanism has been proposed with excellent stability and verified reusability of the proposed photocatalyst.

Keywords Chlorazol yellow · Photocatalyst · Sol–gel method · Adsorption kinetics · Degradation kinetics · Dye degradation · Scavenging effect

Introduction

A new era in the chemical industry was introduced by William Henry Perkin in 1856 with the accidental discovery of the first synthetic dye, mauve (Hübner 2006). Since then, uncountable numbers of dyes have been synthesized, with approximately 10,000 artificial dyes currently servicing the global market (Bazin et al. 2012; Sinha et al. 2013; Gürses et al. 2016). Yearly, about 800,000 tons of dyes are manufactured globally (Jamee and Siddique 2019). And, these dyes possess versatile applications in various branches of the paper, printing, plastic, leather, food, and cosmetics industries, where nearly 80% are being used in textile industries (Asl et al. 2012; Hiremath et al. 2018). Among a wide range of dyes, azo dyes are the most significant and most utilized dyes, which represent more than 60% of the dye family. Roughly 70% of the different types of dyes utilized

---

Communicated by Sami Rtimi.

Zannatul Mumtarin Moushumy and Mohammad Jobaer Hassan have equal contributions.

Highlights
- The TiO_2-5 wt% (Ce-Bi-N) catalyst exhibited photocatalytic degradation of ca. 97% for chlorazol yellow (CY) dye in neutral medium.
- The developed catalyst can destruct CY molecules with a maximum rate of 23.1 μg CY g^{-1} min^{-1}.
- A total of − 25.5 kJ mol^{-1} free energy ($\Delta G^o = -RT\ln K$) was liberated while the catalyst was employed for CY degradation.
- The photodegradation kinetics followed first-order kinetics bellow 23.5 mg L^{-1}, fractional order between 23.5 and 35.0 mg L^{-1}, and zeroth order above 35.0 mg L^{-1} of CY concentration.

✉ Mohammad A. Hasnat
mah-che@sust.edu; mahtazim@yahoo.com

Extended author information available on the last page of the article

Scheme 1 Molecular structure of chlorazol yellow dye

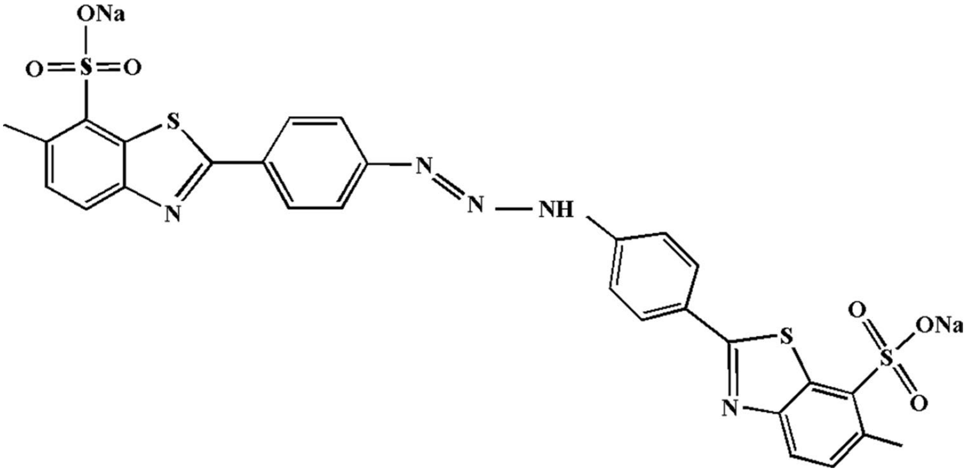

in industries (material, printing, paper fabricating) are azo dyes (Benkhaya et al. 2020).

Every year, during the production of dyes and textiles, just about 140,000 tons of artificial dyes are abandoned in the aquatic systems (DeVito 1993; Slama et al. 2021). The release of color-containing effluents has clear adverse consequences. Intense colors, high pH variations, elevated chemical oxygen demand (COD), and provoked biotoxicity against microorganisms in aquatic systems are some of the consequences created by these effluents (GilPavas et al. 2020; Hasani et al. 2021). Note that even 10–50 mg L^{-1} of water-soluble dyes may have a serious impact on marine organisms (Helmy et al. 2018; Fried et al. 2022), photosynthetic activities, and ecosystems (Çiçek et al. 2007). Moreover, these chemicals are not directly destructed by sunlight, temperature, or microbial attacks and are known to be persistent in nature (Khan et al. 2013; Li et al. 2017; Kishor et al. 2021). Additionally, these chemicals, especially the azo dyes are toxic, mutagenic, and potentially carcinogenic, which is an outright threat to human health and environment (Gičević et al. 2020; Alderete et al. 2021). Chlorazol yellow (CY) is an example of such a dye found in effluents from textile industries (Yaseen and Scholz 2019). CY ($C_{28}H_{19}N_5O_6Na_2S_4$, molecular weight is 695.72 g) is an anionic azo dye containing sulfonic groups. This dye has a complex chemical structure (see Scheme 1), high solubility in aqueous solutions, and high persistence when discharged into the environment. Thus, the treatment of CY dye is a concern in this work.

To eliminate these kinds of dyes from effluents, various physio-chemical strategies like ion exchange centrifugation, coagulation-flocculation, chemical precipitation, sorption, flotation, filtration, sedimentation, and catalytic and sonocatalytic remediation have been developed (Yagub et al. 2014; Nawaz and Ahsan 2014; Yim et al. 2015; Hassani- and Eghbali 2018; Agrawal et al. 2020; Sakr et al. 2020; Liu et al. 2021; Teo et al. 2022). Electrochemical (i.e., ion-oxidation) and biological (i.e., aerobic or anaerobic digestion) techniques are also familiar but have the drawback of sludge generation, which requires expensive solid disposal techniques (Vidya et al. 2016). In this connection, advanced oxidation processes (AOPs) provide powerful oxidizing conditions and are mostly preferred. In AOPs, hydroxyl ions and radicles (having one of the highest oxidative potentials, $E^0 = +2.80$ V) are generated to treat the organic effluents, and then the effluents are entirely degraded to carbon dioxide, water, and some inorganic ions. According to the literature, AOPs utilize photocatalysis, Fenton oxidation, photolysis, ozonation, membrane separation, and etc. for the removal of dye (Danmaliki and Saleh 2017; Alansi et al. 2018; Karim et al. 2022).

However, transition metal-oxide nanoparticles like ZnO, TiO_2, and CeO_2 act as charge carriers during UV/solar irradiation, so they are widely used as photocatalysts (Hasnat et al. 2007; Milosevic et al. 2017; Ani et al. 2018; Milošević et al. 2018; Mishra and Mukhopadhyay 2019; Hassani et al. 2020). There are only a few reports on CY dye degradation using oxide type catalysts, for instance, TiO_2 (Hiremath et al. 2018), α-Fe_2O_3, and γ-Fe_2O_3 (Akrami and Niazi 2016). Scientists consider TiO_2 as the most preferred photocatalyst for wastewater treatment of organic pollutants (Tang and Huren An 1995; Wahi et al. 2005; Uddin et al. 2007; Saadati et al. 2016; Akter et al. 2016; Zeghioud et al. 2019) because TiO_2 semiconductor is cheap, recyclable, stable, corrosion resistant, and light-resistant at ambient conditions. Due to the large energy gap of 3.2 eV, TiO_2-based photocatalytic systems exhibit some limitations in lower efficiency, electron–hole carrier recombination, and photonic yield under visible light (Radoičić et al. 2013). Hence, these facts became the concerns to be mitigated in this study.

Principally, a semiconductor material is activated with the light of a certain wavelength depending on the band gap of that material. The band gap of a semiconductor could be reduced by doping other metals or non-metals.

Applying the advantage of the reduced band gap energy, visible light could be used efficiently and economically instead of UV light in destructing dye molecules. In this regard, elements like N (Ansari et al. 2016; Kovalevskiy et al. 2020), C (Qi et al. 2014; Varnagiris et al. 2019), B (Bilgin Simsek 2017; Niu et al. 2020; Arifin et al. 2022), and S (Cravanzola et al. 2017; Yan et al. 2017) have already been successfully used as dopants of TiO_2. Meanwhile, nowadays, TiO_2 catalysts doped with Ce and Bi dopants are attracting much attention for photochemical treatments. It is reported that decrement of the band gap of the TiO_2 lattice, as well as the increment of the optical absorption in the visible light region, occurs due to the insertion of Ce or Bi particles (Murcia-López et al. 2011; Xue et al. 2011; Li et al. 2014; Worayingyong et al. 2014; Hamdi et al. 2021a). These species not only increase the photocatalytic activity but also prevent electron–hole recombination (Xiong et al. 2015). Moreover, Ce doping provides the scope for the generation of Ce^{3+} and Ce^{4+} via the generation of empty oxygen space on the surface of the catalyst, leading to increased mobility of catalytic particles (Xiong et al. 2015). Besides, Bi doping promotes the feasible photodegradation of organic pollutants under the irradiation of visible light (Pan et al. 2005; Chu et al. 2020).

Considering these issues, a series of Ce, Bi, and N co-doped TiO_2 photocatalysts were prepared by varying the composition of the dopants. Finally, the resultant dopant catalyst termed TiO_2-5 wt% (Ce-Bi-N) was found to show the best catalytic activity under sunlight irradiation. Hence, in this article, the catalytic activity of the TiO_2-5 wt% (Ce-Bi-N) catalyst over CY dye was studied by varying contact time and initial dye concentration. In this study, catalyst selection, adsorption–desorption kinetics, photocatalytic kinetics, and characterizations were performed systematically. The catalyst was characterized using energy-dispersive X-ray spectroscopy (EDX), scanning electron microscope (SEM), X-ray photoelectron spectroscopy (XPS), Fourier-transform infrared spectroscopy (FTIR), and X-ray diffraction (XRD) analysis. The overall experiment was performed on a neutral medium to avoid photocatalytic contamination.

Experimental

Chemicals and reagents

All the reagents used in the experiments were of analytical grade, and used without further treatment. Chlorazol yellow dye ($C_{28}H_{19}N_5O_6Na_2S_4$) was purchased from Philip Harris Limited, Shenstone, England. Titanium (IV) isopropoxide [$Ti(OC_3H_7)_4$], tetra-hydrated cerium sulfate [$Ce(SO_4)_2.4H_2O$], penta-hydrated bismuth nitrate [$Bi(NO)_3.5H_2O$], and urea ($H_2N\text{-}CO\text{-}NH_2$), ethanol ($C_2H_5OH$), and hydrochloric acid (HCl) were bought from Merck, KGaA 64,271 Darmstadt, Germany.

Instruments

To investigate the dye degradation process, a UV–vis spectrophotometer model UV-1800, manufactured by Shimadzu, Japan, was used. The surface morphology of the catalyst was verified using JSM-760F scanning electron microscope (SEM) and for elemental verification, the Oxford INCA 400 energy-dispersive X-ray spectroscope (EDX) was used. Powder X-ray diffractometer (XRD) patterns were recorded on a fully automatic horizontal multipurpose X-ray diffractometer (Rigaku Smartlab; Rigku Corp.) as a 2θ range from 20 to 90°. The metal-oxide bonding was confirmed via Fourier-transform infrared spectrophotometer (IRAffinity-1, Shimadzu, Japan). The X-ray photoelectron spectra (XPS) study was performed using the delay-line detector (DLD) spectrometer (Kratos Axis-Ultra, Kratos Analytical Ltd.) with an Al Kα radiation source of 1486.6 eV. Component separation and energy calibration were done with the bundled software where pure Gaussian profiles were maintained with a linear background.

Preparation of the photocatalyst

The preparation process of the photocatalyst powder was carried out following the processes described by Wei et al. (2013) with some modifications (see supplementary information of Scheme S1). Firstly, to prepare solution A, 32.5 mL of ethanol (C_2H_5OH) was taken as a solvent in a 250-mL round-bottom flask. As a precursor, 4 mL of titanium tetra-isopropoxide ($Ti[OCH\ (CH_3)_2]_4$) was added dropwise. The molar ratio or the volume ratio of solution A was 42:1 or 32.5:4, respectively. Then, solution A was stirred vigorously for 10 min.

Next, for solution B, 32.5 mL of ethanol, 5.3 mL of HCl, and 0.5 mL of H_2O (at 42:4.8:2 molar ratio or 32.5:5.3:0.5 volume ratio) were mixed into a 100-mL beaker. At this point, solution B was transferred to solution A with vigorous stirring for 10 min. Then, 0.1505 g of $CeSO_4.4H_2O$, 0.1210 g of $Bi(NO_3)_2.5H_2O$, and 0.1120 g of $H_2N\text{-}CO\text{-}NH_2$ were added sequentially to the mixture for 5% doping of Ce, Bi, and N. After mixing, the resultant solution was sonicated for 10 min. Finally, the mixture was vigorously stirred for 2 h at room temperature before being kept for 24 h for aging. Consequently, the solution became transparent after aging.

Then, the solutions were transferred into a beaker and dried at 100 °C. The dried samples were calcined for 2 h at 200 °C and another 2 h at 500 °C using a muffle furnace (JSMF-30 T, Korea) to remove all organic pollutants. Later, the powder was cooled down gradually in the muffle furnace for 12 h at room temperature. Finally, TiO_2-5 wt% (Ce-Bi-N) formed as the doped catalyst, which would be exploited in photocatalytic degradation.

Photocatalytic degradation

To attain adsorption–desorption equilibrium, 0.250 g of TiO_2-5 wt% (Ce-Bi-N) photocatalyst powder was added into 50 mL of 5 mg L^{-1} CY solution and the rest was kept in dark treatment for 40 min. Every 5 min, 3.0 mL of the aliquot of solution under dark treatment was collected and the absorbance was measured at 388 nm to confirm CY adsorption on the catalyst surface. While absorbance was found unchanged due to the establishment of adsorption–desorption equilibrium, the solution was then kept under sunlight irradiation for 120 min in the daytime (preferably between 10:00 am and 1:00 pm). Periodically, the absorbance of the solution under photolysis was measured at 388 nm to ensure photocatalytic degradation of CY dye molecules.

The percentage of CY degradation at a time t was calculated by using the following relationship.

$$\%\text{CYdegradation} = \frac{C_0 - C_t}{C_0} \times 100 \tag{1}$$

where C_0 (mgL^{-1}) and C_t (mgL^{-1}) are the initial and desired time intervals of the liquid phase concentrations of CY, respectively.

Results and discussion

Characterization of TiO_2-5 wt% (Ce-Bi-N) catalyst

Although a series of compositionally varied Ce, Bi, and N-doped TiO_2 catalysts were prepared, TiO_2-5 wt% (Ce-Bi-N) showed the best photocatalytic activity (discussed in the later sections); hence, critical characterizations were made for this catalyst only. First, to obtain the morphological information of TiO_2 and TiO_2-5 wt% (Ce-Bi-N) nanocomposite, SEM images were recorded. The surface morphology shown in Fig. 1A and Fig. 1B represents SEM images of TiO_2 and TiO_2-5 wt% (Ce-Bi-N) nanocomposite, respectively. Comparing these images, it can be stated that the morphology of the TiO_2-5 wt% (Ce, Bi, N) nanocomposite powder is comparatively more uniform than that of TiO_2 powder and many of the pores left in TiO_2 are blocked by the dopant particles.

It is apparent from Fig. 1B that the doping of 5 wt% (Ce, Bi, N) occurred significantly in TiO_2 powder due to the facilitation of smaller grain sizes or the crystal size of the nanocomposite. On a further note, for the elemental confirmation of the TiO_2-5 wt% (Ce-Bi-N) photocatalyst, EDS analysis was performed to justify the presence of Ti, O, Ce, Bi, and N (see Fig. 1C) with the atomic percentage of the elements (see supplementary information of Table S1). Here, the as-synthesized photocatalyst image

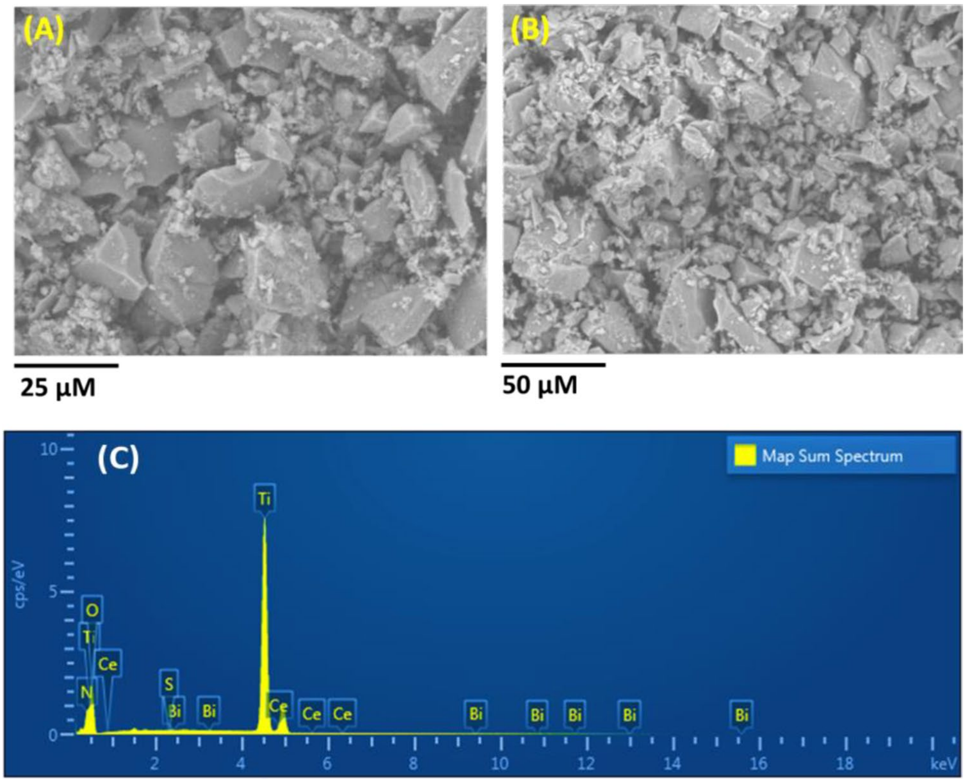

Fig. 1 (**A**) SEM image of TiO_2 particles. (**B**) SEM image of TiO_2-5 wt% (Ce-Bi-N) photocatalyst. (**C**) EDS spectrum of TiO_2-5 wt% (Ce-Bi-N) photocatalyst

shown in Fig. S1A is the uniform entity of the individual elements demonstrated in Fig. S1B to Fig. S1F.

Next, XRD patterns of the doped and undoped TiO_2 catalyst were recorded to examine the altered crystalline properties. The PXRD patterns of TiO_2 and TiO_2-5 wt% (Ce, Bi, N) shown in Fig. 2 exhibit several peaks such as (101), (004), (200), (105), (211), (204), (116), (220), (215), and (303) indexing of the anatase phase of TiO_2 [53].

It is remarkable that similar peaks at similar positions were obtained in both cases. Moreover, no additional peaks related to Ce, Bi, and N appeared for the TiO_2-5 wt% (Ce-Bi-N) spectral pattern, which indicates that Ce, Bi, and N acted just as dopants and did not change the crystalline structure of the catalyst (Shi et al. 2010). Crystallite sizes of TiO_2 and TiO_2-5 wt% (Ce-Bi-N) were calculated as 16.1562 nm and 9.6730 nm, respectively, using the well-known Scherer equation given in Eq. (2).

$$D = \frac{K\lambda}{\beta\cos\theta} \tag{2}$$

Here, D denotes the crystallite size (nm), λ is the wavelength of the X-ray sources (0.15406 nm), K is the Scherrer constant (0.9), β is the full width at half maximum (radians), and θ is the peak position (radians). The smaller crystallite size of TiO_2-5 wt% (Ce-Bi-N) (9.6730 nm) than that of TiO_2 (16.1562 nm) is attributed to the wider peak and lower intensity of TiO_2-5 wt% (Ce-Bi-N) than that of TiO_2.

Next, FTIR spectra were recorded before and after the doping of the dopant particles to verify the metallic bonding of the catalyst. From Fig. 3A, it is evident that the peak at 3272 cm^{-1} corresponds to the O–H stretching vibration band of the moisture, whereas the peak at 1615 cm^{-1} represents the bending vibration band of O–H for adsorbed H_2O and the peak at 550 cm^{-1} represents the stretching vibration band of Ti–O-Ti (Liu et al. 2012; Sarker et al. 2022).

Meanwhile, after the doping of Ce, Bi, and N onto TiO_2, three new peaks creep out, as can be seen in Fig. 3B. Along with the basic peaks of TiO_2 catalyst, the peak at 1050 cm^{-1} can be assigned to the stretching vibration band of Bi-O-Ti (Astuti et al. 2021), the peak at 1120 cm^{-1} can be assigned to the Ce–O-Ti stretching vibration band, and finally, the peak at 1172 cm^{-1} is the O-N-Ti stretching vibration band (Huang et al. 2018). So, it can be ascertained from the signature of the metallic bonding that Ce, Bi, and N were successfully incorporated into the TiO_2 matrix.

For further verification, X-ray photoelectron spectra (XPS) were recorded to characterize the nature of chemical bonds in the developed catalyst. Figure 4 represents the XPS analysis of as-synthesized TiO_2 powder.

The survey scan shown in Fig. 4A reveals the presence of Ti and O in the synthesized material. Figure 4B exhibits the XPS spectra of Ti 2p, which contains two major peaks. The binding energies of these two peaks are 458.3 eV and 464.0 eV, which represent Ti $2p_{3/2}$ and Ti $2p_{1/2}$, respectively. Here, these peaks are for the presence of Ti^{4+} in the TiO_2 lattice (Bharti

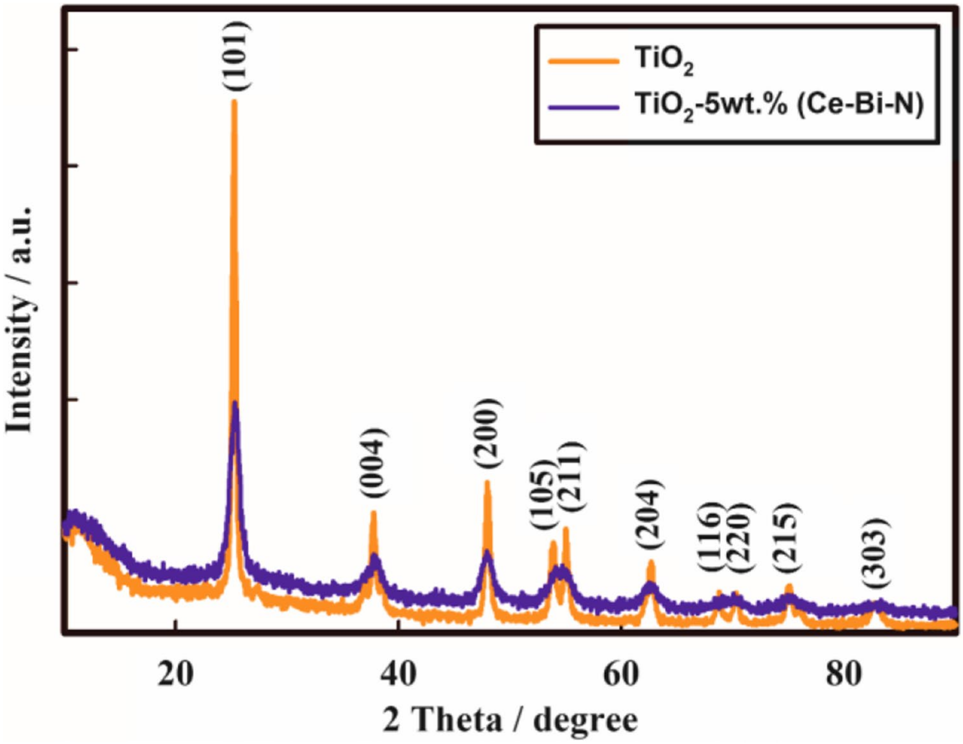

Fig. 2 XRD spectra of TiO_2 and TiO_2-5 wt% (Ce-Bi-N) photocatalyst

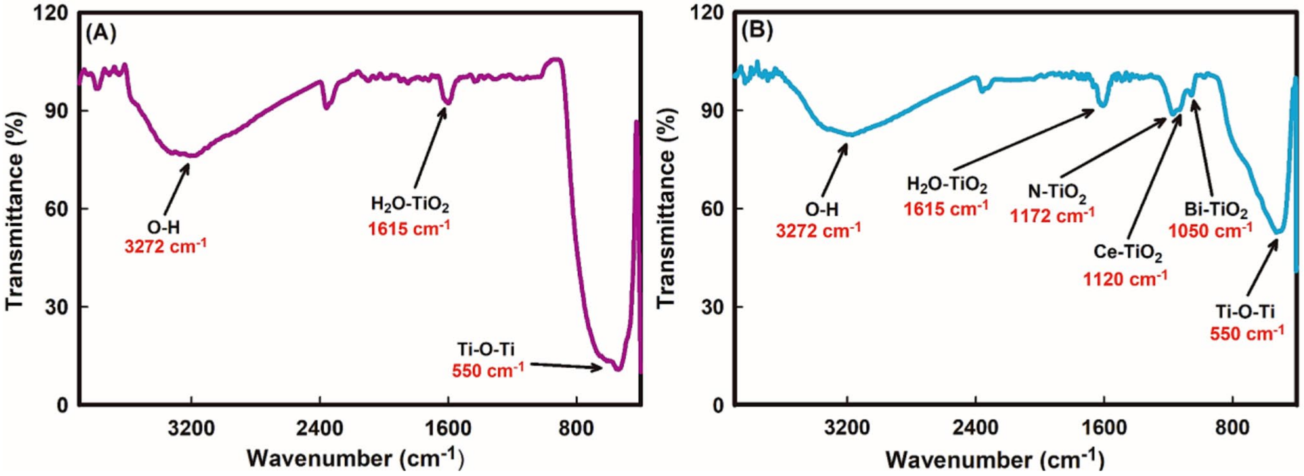

Fig. 3 FTIR spectra of the metallic bonding of (**A**) TiO_2 and (**B**) TiO_2-5 wt% (Ce-Bi-N) photocatalyst

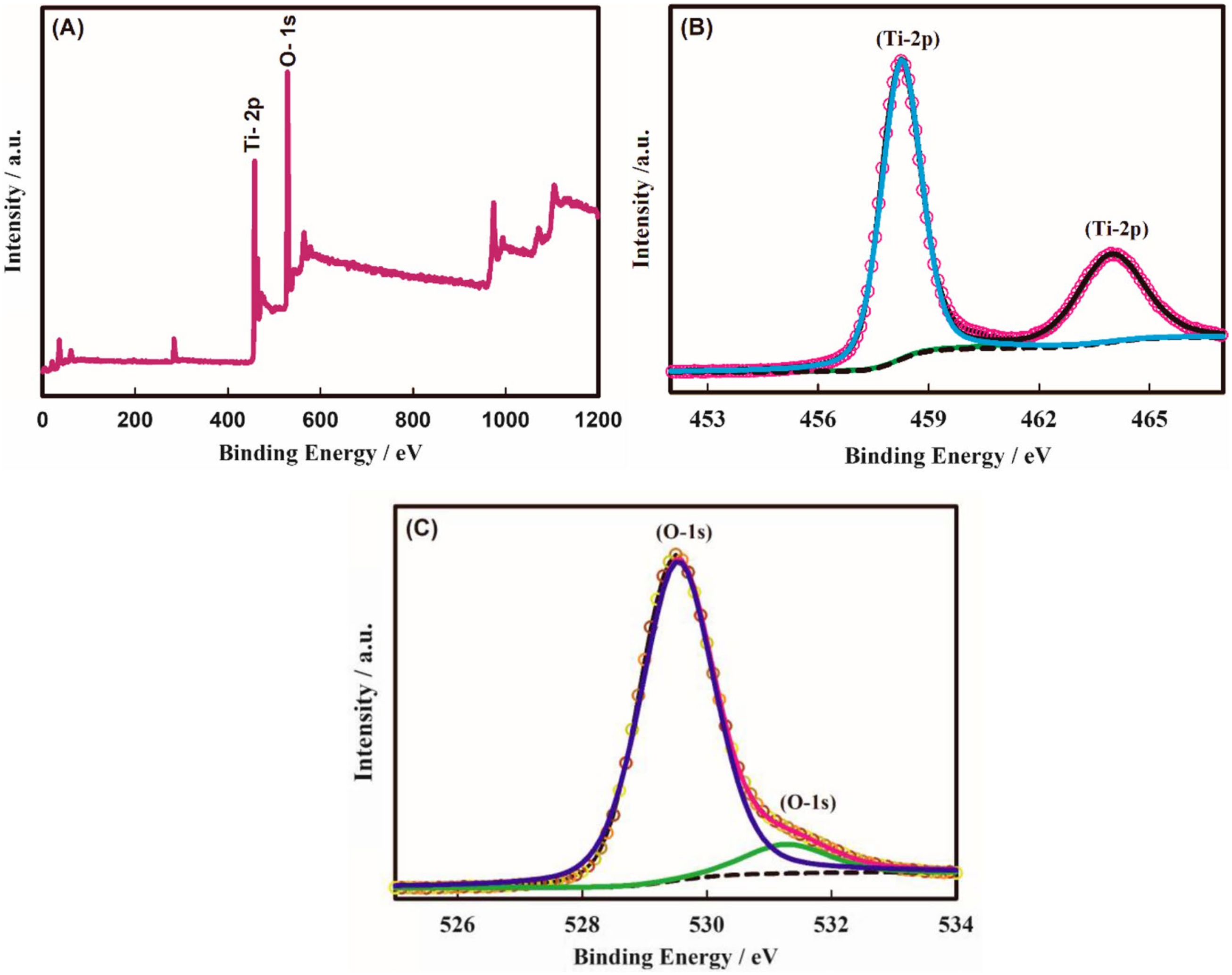

Fig. 4 XPS analysis of TiO_2. (**A**) Survey scan. (**B**) Ti 2p. (**C**) O 1s XPS spectra

et al. 2016). The binding energy difference of 5.7 eV for these two peaks further proved the formation of TiO_2. From Fig. 4C, the deconvolution of the O 1s peak revealed two peaks at the binding energies of 529.5 eV and 531.3 eV for Ti–O and O–H, respectively (Bharti et al. 2016; Yu et al. 2017). The peak intensity of the Ti–O bond is quite high compared to the O–H bond, which attributes to the formation of TiO_2. The XPS analyses of TiO_2 doped with Bi, Ce, and N are presented in Fig. 5.

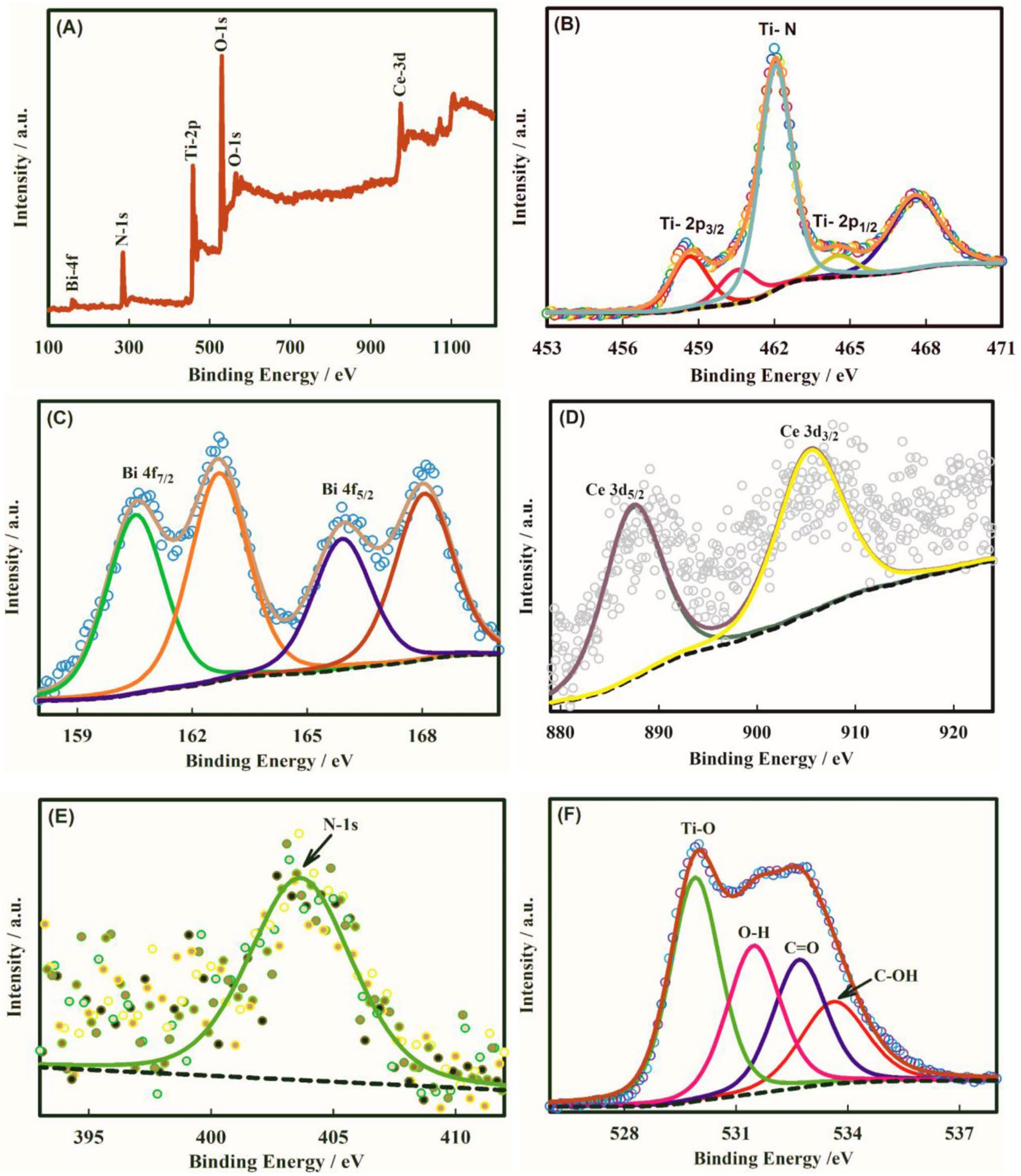

Fig. 5 XPS analysis of TiO_2-5 wt% (Ce-Bi-N). (**A**) Survey scan. (**B**) Ti 2p. (**C**) Bi 4f. (**D**) Ce 3d. (**E**) N 1 s. (**F**) O 1s XPS spectra

Herein, from Fig. 5A, a survey scan confirms the presence of Bi, Ce, and N in the TiO_2 moiety. The Ti 2p spectra deconvolution yielded five peaks, which are shown in Fig. 5B. Two peaks at binding energies of 458.6 eV and 464.5 eV are for Ti^{4+} in Ti $2p_{3/2}$ and Ti $2p_{1/2}$, respectively (Bharti et al. 2016). Another peak at 462.0 eV is assigned to the Ti-N bond (Wang et al. 2017). Small peaks were found at 460.5 eV, attributed to Ti^{3+} (Zhu et al. 2017). The peak at 467.6 eV represents the Bi $4d_{3/2}$ overlapped with the Ti 2p XPS spectra (Luo et al. 2019). The Bi 4f XPS spectra can be seen in Fig. 5C, where fitting data revealed four peaks**.** Two well-separated peaks at 160.5 eV and 165.9 eV refer to Bi $4f_{7/2}$ and Bi $4f_{5/2}$ accordingly. These peaks are assignable to Bi^{5+} (Chen et al. 2013), whereas the peaks at 162.7 eV and 168.0 eV can be assigned to basic nitrate impurities (Abdullah et al. 2012). Figure 5D represents the Ce 3d XPS spectra where the deconvolution of this spectra provides two peaks at 905.4 eV and 887.4 eV, corresponding to Ce $3d_{3/2}$ and Ce $3d_{5/2}$ in Ce^{3+} (Abdullah et al. 2012). In Fig. 5E, the N 1s XPS peak at 403.7 eV is formed due to the surface nitrites (NO_2^-) (Ozensoy et al. 2005). The presence of fewer species on the photocatalyst may very well be the reason of the modest signals of the dopants in Fig. 5D and 5E. As shown in Fig. 5F, fitting the data of O 1s revealed four peaks**.** The peaks at 529.9 eV, 531.5 eV, 532.7 eV, and 533.6 eV correspond to Ti–O, O–H, C = O, and C–OH, respectively. Here, the O–H bond might be formed by moisture, while the C = O and C–OH bonds could be formed by the urea, which is essentially employed as a supply of nitrogen (Bharti et al. 2016; Jang and Hwang 2018; Ferreira et al. 2019). From the overall XPS analysis, the calculated percentages of Bi, Ce, and N were found to be 2.8%, 6.8%, and 0.5%, respectively.

Photocatalytic activity

Selection of catalyst

It is accepted that anatase TiO_2 is a highly efficient photocatalyst in attaining dye degradation under UV irradiation. However, this catalyst does not efficiently work under visible light conditions because of its higher band gap energy of 3.20 eV. Thus, to make this catalyst workable even under sunlight, in this research, we have synthesized a series of photocatalysts by doping different combinations of Ce, Bi, and N into the core of TiO_2 particles. The photocatalytic activities of the synthesized photocatalysts pertaining to CY degradation are tabulated in Table 1. In each case, to perform photocatalytic activity, 50 mL of reaction mixture was prepared with 0.250 g of the photocatalyst where the CY dosage was 5 mg L^{-1}. Initially, the resultant mixture was kept in the dark for 60 min under stirred conditions. Assuming that within this time, an adsorption–desorption equilibrium is reached, the reaction mixture was kept for 120 min under sunlight for photolysis. To monitor the concentration changes, spectral changes between 200 and 800 nm were recorded periodically. From Figure S2 of the supplementary information, it is seen that CY molecules exhibit an absorption band at 388 nm due to the π-π* transition. At the end of the photolysis with TiO_2-5 wt% (Ce-Bi-N) [termed as C7] catalyst at 120 min, this band is diminished, indicating almost complete degradation. It can be noted that at 120 min, a pure TiO_2 catalyst attained 66.22% CY degradation, whereas the C7 catalyst obtained 97.18% degradation, which is the maximum in comparison to other catalytic compositions as reported in Table 1. The reason behind the improved catalytic performance can be primarily credited to the possible lowering of the band gap energy of the developed catalyst (Breault and Bartlett 2012; Modwi et al. 2018). Later, the specific catalytic efficiency was also estimated at ca. 98% for the C7 catalyst using the analogous Eq. (1).

Table 1 Photocatalytic activity of different combinations of dopants in TiO_2 nanoparticles for the degradation of CY dye molecules

Catalyst code	Photocatalysts	Band gap (E_g)/eV	% CY degradation
C1	TiO_2	3.20	66.22
C2	TiO_2-5 wt% Ce	3.13	68.06
C3	TiO_2-5 wt% Bi	3.12	67.31
C4	TiO_2-5 wt% N	3.14	67.12
C5	TiO_2-5 wt% (Ce-Bi)	3.06	74.35
C6	TiO_2-5 wt% (Ce-N)	3.09	71.14
C7	TiO_2-5 wt% (Ce-Bi-N)	2.63	97.18

Catalyst dosage 5 gL^{-1}, [CY] = 5 mg L^{-1}, pH ~ 7, temp. = 25 °C, stirring rate = 100 rpm

However, to unveil the reason for such improved catalytic performance, band gap energies of all-catalytic compositions were evaluated as the band gap is directly related to the dye degradation capacity of any photocatalyst (Khan et al. 2014; Hemalatha et al. 2016). It is accepted that the higher the band gap, the higher the electron–hole separation between the valance band (VB) and the conduction band (CB). In such conditions, it is impossible to degrade the dye molecules under sunlight irradiation. Consequently, an attempt was made to narrow the band gap of TiO_2 (3.20 eV) by using metal and non-metal dopants. To do this, suspensions of the catalysts having a concentration of 5 g L^{-1} were prepared and UV–visible spectra were recorded. The Tauc plot (in Eq. (3)) (Tauc et al. 1966) was used to determine the band gap of developed catalysts.

$$\alpha h\upsilon = A\left(h\upsilon - E_g\right)^n \tag{3}$$

Here, α and $h\nu$ indicate the absorption coefficient and photon energy, respectively. A indicates the absorbance of the material, E_g indicates the material's band gap energy, and n indicates the nature of the optical transition. In this case, n was set to 2 for the direct allowed transition. The adjustment of spectral data with the Tauc equation for different catalytic suspensions is shown in Fig. 6B, and the original light absorption of the catalyst is manifested in Fig. 6A.

As expected, it is seen from Table 1 that the incorporation of metal and non-metal dopants such as Ce-Bi-N by 5 wt% into the TiO_2 catalytic matrix declined the E_g value of the TiO_2 catalyst to a minimum value of 2.63 eV from its original value of 3.20 eV. However, incorporation of only Ce or Bi or N or even their binary combinations could not exceed the minimum E_g value obtained by the C7 catalyst. This observation suggests that the highest catalytic performance could be attained while all the Ce, Bi, and N species are doped into the TiO_2 catalyst's matrix. However, there may remain confusion about the other compositions of the quaternary catalyst TiO_2-Ce-Bi-N that could show the best catalytic performance. To dispel this confusion, another series of catalysts were prepared by varying the percentage of Ce-Bi-N species. The photocatalytic performances of TiO_2-Ce-Bi-N catalysts of variable compositions are reported in the supplementary information of Table S2. The evaluation of E_g values of all-catalytic compositions is shown in the supplementary information of Fig. S2B derived from the UV plot of Fig. S2A.

It is perceptible that the best catalytic performance pertaining to CY degradation could be attained while all the dopants such as Ce, N, and Bi are equally present by 5% in the TiO_2 matrix. As the C7 catalyst exhibited the best catalytic performance, the rest of the studies were performed using this catalyst only.

Adsorption–desorption equilibrium

The present research aims to attain CY degradation with a composite catalyst using sunlight irradiation. As the C7 catalyst exhibited catalytic superiority, hence, it is important to unveil the time of adsorption–desorption equilibrium such that available sunlight irradiation can be applied in the daytime. To do this, 50 mL of 5 mg L^{-1} of CY solution was prepared in the presence of the C7 catalyst at pH ~ 7.0 and kept in the dark. As time progressed, CY molecules started to be adsorbed on the surface of catalyst particles. Consequently, the CY concentration gradually decreased, as demonstrated by the lowering of absorbance at 388 nm in Fig. 7A. The amount of CY adsorbed (q_t) was determined from the spectral data using Eq. (4).

$$q_t = \frac{A_o - A_t}{\varepsilon} \tag{4}$$

where A_o and A_t are the absorbances at 388 nm and ε represents the molar extinction coefficient of CY dye (3.18×10^{-2} L mg^{-1}).

Figure 7B shows the q_t vs. time plot for CY adsorption onto the C7 catalyst. It is apparent from this figure that the amount of CY adsorption gradually increased with the passage of time and reached a maximum at 30 min. After this time, no measurable changes in the CY spectrum were noticed. This observation suggests that under the experimental condition, at least a period of 30 min is required to reach adsorption–desorption equilibrium prior to photolysis under any kind of irradiation.

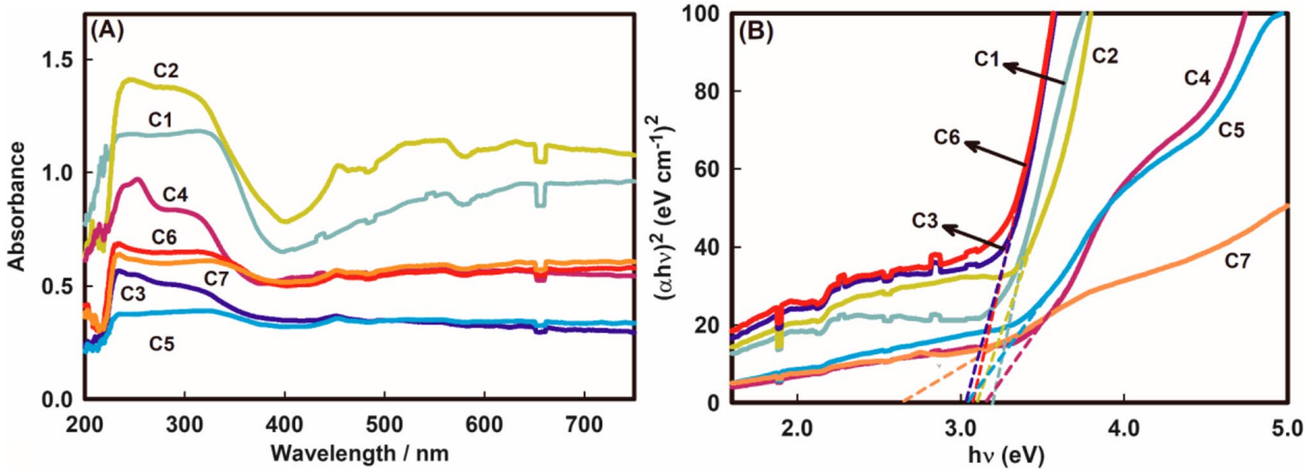

Fig. 6 (**A**) UV–visible spectra of CY dye degradation by TiO_2 photocatalyst with various dopants (catalyst codes mentioned in Table 1). (**B**) Tauc plot of TiO_2 photocatalyst with various dopants. Catalyst dosage: 5 mg L^{-1}, [CY] = 5 mg L^{-1}, pH ~ 7, temp. = 25 °C, stirring rate = 100 rpm

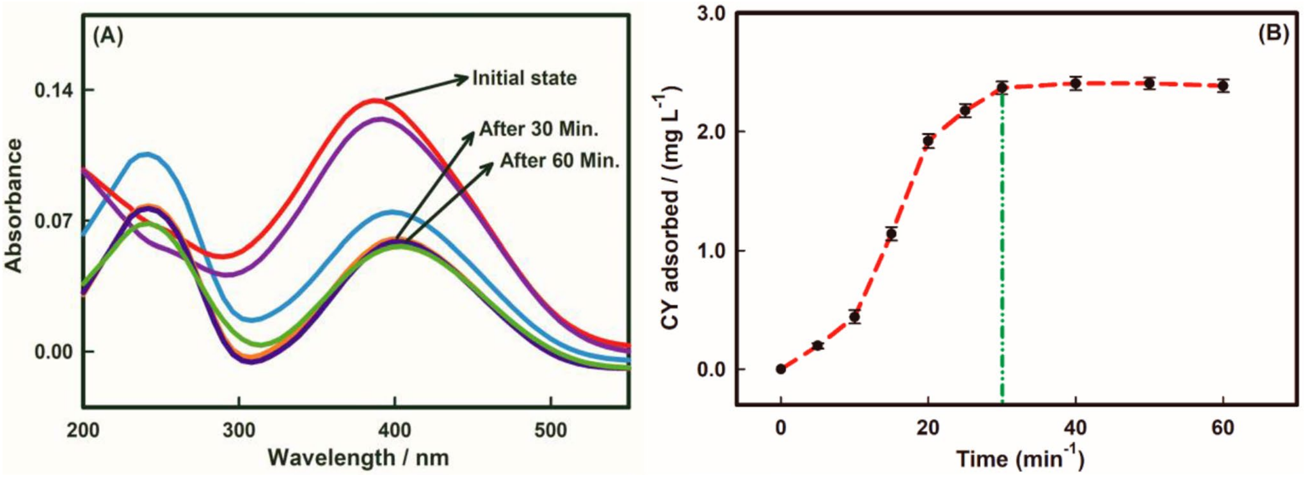

Fig. 7 (**A**) UV–visible spectra of CY adsorption onto the C7 catalyst in the dark and (**B**) a plot of the dye adsorption with respect to time. Catalyst dosage: 5 g L^{-1}, [CY] = 5 mgL^{-1}, pH ~ 7.0, temp. = 25 °C, stirring rate = 100 rpm

At this point, the adsorption kinetics of the CY dye on the C7 catalyst was evaluated by using the pseudo-first-order and the pseudo-second-order kinetics models (Caner et al. 2009; Kalantary et al. 2015). Lagergren described the pseudo-first-order kinetics model as per Eq. (5),

$$\ln\left(1 - q_t/q_t\right) = -k_1 t \tag{5}$$

where q_e and q_t refer to the amount of CY dye adsorbed (mg g^{-1}) at equilibrium, and t (min) refers to the adsorption time progressed, respectively. k_1 (min^{-1}) is the equilibrium rate constant of pseudo-first-order adsorption, which was calculated from the slope of ln $(1 - q_t/q_e)$ vs. t curve as shown in the supplementary information of Fig. S4A. The values of k_1 and the correlation coefficient R^2 were 0.2036 min^{-1} and 0.84, respectively. In the case of a pseudo-second-order kinetics model for the CY dye adsorption process, Eq. (6) can be used.

$$\frac{t}{q_t} = \frac{1}{k_2 q_e^2} + \frac{1}{q_e} t \tag{6}$$

Here, k_2 indicates the rate constant at equilibrium of the pseudo-second-order adsorption (min g mg^{-1}) which was calculated using the slope and the intercept of the curve as in the supplementary information of Fig. S4B. The values of k_2 and the correlation coefficient R^2 were 0.6638 (g mg^{-1} min^{-1}) and 0.95, respectively. From the above investigation, it was found that the R^2 value of pseudo-first-order kinetics (0.84) was lower than that of pseudo-second-order kinetics ($R^2 = 0.95$), which corroborated that the adsorption process of CY dye onto C7 catalyst followed the pseudo-second-order kinetics model.

Degradation kinetics

In order to optimize the C7 catalyst's degradation capacity, CY concentration-dependent photocatalytic degradation experiments were performed for 120 min under sunlight irradiation between 11.00 am and 1.00 pm on a sunny day. In this case, the CY concentration was varied from 0 to 45 mg L^{-1}, keeping the catalyst dose constant at 5 g L^{-1}. By measuring the changes in CY concentration with respect to irradiation time, the rate of CY (v) degradation was determined as per Eq. (7).

$$v = -\frac{1}{5}\frac{d[CY]}{dt} \tag{7}$$

Figure 8 shows the variation of the CY degradation rate (v) with CY concentration. It is noticeable that the

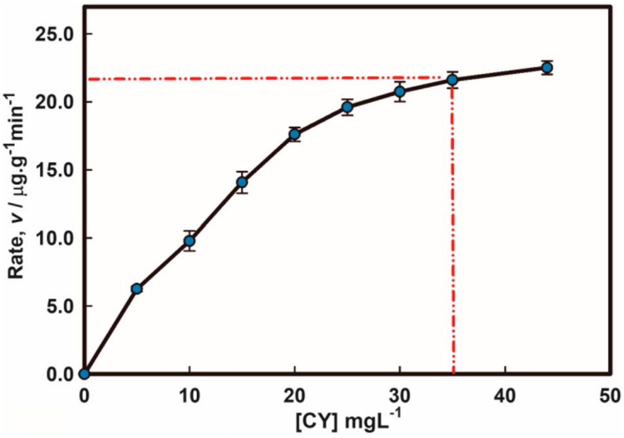

Fig. 8 Dependency of CY degradation rate on fixed C7 catalyst dose. pH ~ 7, temp. = 25 °C, stirring rate = 100 rpm

degradation rate decreased with the increment of CY concentration. This observation suggests that photons of sunlight destructed CY molecules adsorbed on C7 catalyst particles. At the same time, free CY molecules diffused to the catalyst's surface to start another cycle of reaction followed by adsorption. However, as the CY concentration reached ca. 35 mg L^{-1}, the degradation rate became limited to a value of 23.1 μg CY g^{-1} min^{-1}, and further increments of CY concentration did not improve the degradation rate any more. This observation suggests that at this concentration of CY, the surface of the C7 catalyst became highly saturated with the adsorbed CY molecules where the adsorption rate and the degradation rate became equal. Moreover, as the catalyst concentration was fixed, the photoactive species, such as evolved hydroxyl radicals ($OH^{\bullet}$) and superoxide (O_2^-), were also fixed in number (Hemalatha et al. 2016). The degradation rate reached a maximum at higher concentrations of CY dye because the number of oxidants required to degrade the dye was not sufficient. For the same reason, further concentration effects were not observed. Thus, it can be considered that the C7 can degrade CY molecules with a maximum rate of 23.1 μg g^{-1} min^{-1}.

However, surface-confined reaction kinetics could be best explained by the surface coverage of CY molecules on the C7 catalyst. If θ is the surface coverage of CY molecules on the C7 catalyst, then based on the Langmuir adsorption isotherm (Hasnat et al. 2007), θ could be related to the adsorption equilibrium constant (K) and the corresponding CY concentration [CY] by Eq. (8);

$$\theta = \frac{K[\text{CY}]}{1 + K[\text{CY}]} \quad (8)$$

Under photolysis, adsorbed CY molecules undergo degradation; hence, the photocatalytic degradation rate (v) must be proportional to the value of θ. Consequently, the CY degradation rate could be expressed by Eq. (9) where k is the proportionality constant.

$$v = k\frac{K[\text{CY}]}{1 + K[\text{CY}]} \quad (9)$$

The linearization of Eq. (9) yields Eq. (10) given as follows.

$$\frac{1}{v} = \frac{1}{kK[\text{CY}]} + \frac{1}{k} \quad (10)$$

It is already reported that above 35 mg L^{-1} CY concentration, the photocatalytic degradation rate was found to be independent of CY concentration. This means that above this concentration, the surface of the C7 catalyst becomes saturated with adsorbed CY molecules, i.e., at this concentration, θ equals unity. Hence, according to Eqs. (9) and (10), CY degradation should follow zeroth order kinetics above 35 mg L^{-1} CY concentration. It is worth noting that according to Eq. (9) at sufficiently low CY concentration i.e., while $1 >> K[\text{CY}]$, the degradation kinetics should follow first-order kinetics. Thus, it was necessary to evaluate the value of K. For this purpose, $1/v$ was plotted against 1/[CY] within the CY concentration range between 5 and 32 mg L^{-1} as shown in Fig. 5.

From the slope and intercept of Fig. 9, the values of k and K were evaluated as 2.42×10^{-7} min^{-1} and 2.95×10^4 mol L^{-1}, respectively. This parametric evaluation suggests that the product of K and [CY] equals unity while [CY] value equals 3.39×10^{-5} M or 23.5 mg L^{-1}, implying that below this concentration, the CY degradation follows first-order kinetics. By contrast, the reaction order was fractional between 23.5 and 35.0 mg L^{-1} of CY concentration. Finally, concerning thermodynamics, the evaluation of K value assumes that − 25.5 kJ mol^{-1} free energy ($\Delta G^o = -RT\ln K$) was liberated while the C7 catalyst was employed for CY degradation under experimental conditions.

Degradation mechanism

At this stage, the photodegradation mechanism of CY molecules can be summarized by the fact that CY degradation is initiated by the absorption of light that is equal to or greater than the band gap of the semiconducting photocatalyst. The photodegradation phenomenon, as shown in Scheme 2, is based on the ease of migration of electrons (ejected on sunlight irradiation) from the valance band to the conduction band. Electrons are promoted to the conduction band (CB) from the valence band (VB) by creating a hole in the valance band followed by Eq. (11). These electron holes ($e^- - h^+$) react with electron acceptor and electron donor species which are adsorbed on the photocatalyst surface. The VB and the CB energies were calculated and presented in the

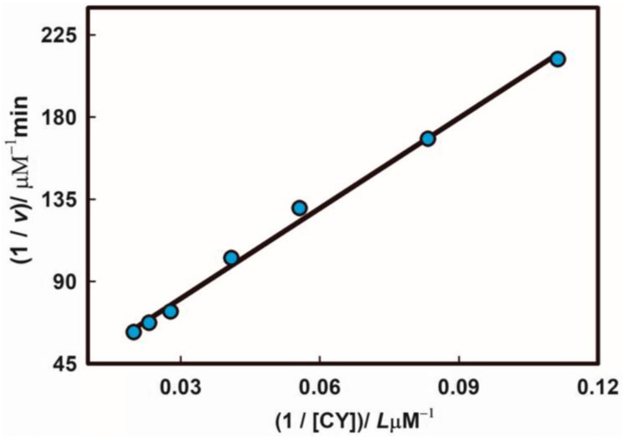

Fig. 9 A plot of 1/v against 1/[CY]. Catalyst dosage: 5 gL^{-1}, pH ~ 7.0, temp. = 25 °C, stirring rate = 100 rpm

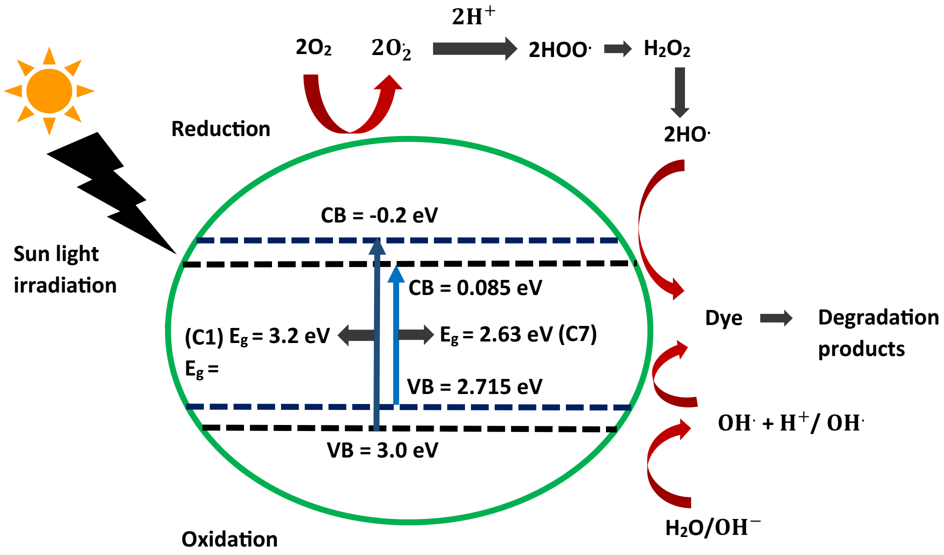

Scheme 2 Proposed photocatalytic degradation mechanism for CY dye. Working conditions: catalyst dosage: 5 g L^{-1}, [CY] = 5 mg L^{-1}, pH ~ 7.0, temp. = 25 °C, stirring rate = 100 rpm

scheme from the following formulas (Hu et al. 2011; Ali et al. 2021).

$$E_{CB} = \chi_s - E_e - 0.5E_g \tag{11}$$

$$E_{VB} = E_{CB} + E_g \tag{12}$$

where E_{CB} and E_{VB} imply the CB and VB band potentials, which specifies the absolute electronegativity of the semiconductor, and Ee and Eg imply the energy of free electrons on hydrogen scale (4.5 eV) and band gap energy of semiconductor, respectively. Herein, the estimated χ value for C1 and C7 catalysts was 5.90 (Hu et al. 2011; Ali et al. 2021). The E_{CB} values of C1 and C7 were then determined to be − 0.2 eV and 0.085 eV vs. NHE, respectively. Furthermore, the E_{VB} values for C1 and C7 catalysts were determined to be about 3.0 eV and 2.715 eV vs. NHE, respectively. Following this rapid and enhanced photocatalytic activity of the C7 catalyst, the mechanism of CY photodegradation is proposed in Scheme 2.

Reactive oxygen species (ROS), namely superoxide (O_2^-), hydroxyl radicals ($OH^{\bullet}$), and photogenerated holes (h^+), play a key part in photocatalytic degradation reactions. Therefore, trapping the ROS by scavenging agents like ethanol, glycerol, benzoquinone (BQ), and EDTA is typically used to justify the role of these species in photocatalytic degradation (Zeghioud et al. 2019). To examine the impact of the inhibition using scavenging agents, an initially blank effect was observed without any scavengers. Later, the degradation efficiency was examined thoroughly using the scavenging agents, and the outcome showed a noticeable effect, as shown in Fig. S5 of the supplementary information. Herein, it is obvious that the presence of scavengers reduced the degradation efficiency of the C7 catalyst, which implies the existence of ROS in the degradation as well. And it is to mention that the hole scavengers (glycerol and EDTA) had negligible effect in degradation. In fact, when the scavengers trapped the holes, electrons were allowed to be freed and consequently generated superoxide by reacting with O_2 as given in Eq. (14). Later, the generated O_2^- reacts with the surrounded water (H_2O) to produce peroxide and hydroxyl ions (OH^-) following Eqs. (15) and (16). Rationally, it can be inferred from the other scavenging (BQ and ethanol) effects that the superoxide and hydroxyl radicals have significant functionality in the overall CY dye degradation (Liu et al. 2017). Basically, superoxide (O_2^-) and hydroxyl radical ($OH^{\bullet}$) are strong oxidizing agents and oxidize organic dyes such as CY and lead to harmless dye degraded products (Eq. (17)), which could tentatively be CO_2, NO_2, SO_2, H_2O, and etc. (Vidya et al. 2020). The reaction mechanism is as follows (Eqs. (13)-(17)),

$$C7 + hv \rightarrow C7\left(e_{CB}^- + h_{VB}^+\right) \tag{13}$$

$$e_{CB}^- + O_2 \rightarrow O_2^- \tag{14}$$

$$O_2^- + 2H_2O \rightarrow H_2O_2 + O_2 + 2OH^- \tag{15}$$

$$H_2O_2 + e_{CB}^- \rightarrow OH + OH^- \tag{16}$$

$$C7 + O_2\left(O_2^- \mathrm{or} OH\right) \rightarrow \mathrm{dyedegrationproducts} \tag{17}$$

Based on these findings, it can be stated that O_2^- had a principal role in the degradation where as $OH^{\bullet}$ radical had an auxiliary support in the photodegradation.

Reusability, stability, and comparative study

In general, the reusability of a photocatalyst has imperative importance for practical applications. Following this, a series of experiments were conducted using the proposed C7 catalyst for the purpose of CY degradation under sunlight irradiation. The experiments were carried out for four consecutive times and the noted degradation efficiencies are manifested in Fig. 10A. Herein, after the completion of the first experiment, the catalyst was recovered, rinsed, and dried for a certain time; then, it was further reused in a fresh solution of CY dye, maintaining the as-used experimental conditions. The reason for the reduction of the degradation efficiency after consecutive experiments could either be the blocking of active sites with the adsorption of CY or could be the system loss during the recovery and reuse of the photocatalyst (Hassani et al. 2020).

Just after the reusability test, FTIR spectra were recorded to observe the stability of the composite photocatalyst, as can be seen from Fig. 10B. And it is pretty clear from the spectra that the photocatalyst remained stable even after four consecutive degradations with a slight negligible shift.

Afterwards, a comparison of the proposed catalyst is made against various TiO_2-based photocatalysts as shown in Table 2. In comparison, the proposed catalyst has clearly outperformed efficient photocatalytic activity toward CY dye in natural sunlight irradiation, making it a viable and competent photocatalyst for industrial wastewater purification.

Conclusion

A 5 wt% of Ce-Bi-N co-doped TiO_2 composite catalyst was prepared through a simple sol–gel method for the efficient treatment of wastewater laced with dyes such as chlorazol yellow. When exposed to sunlight, the proposed catalyst exhibited photocatalytic degradation of ca. 97% for CY dye at neutral medium (pH ~ 7). Despite reaching

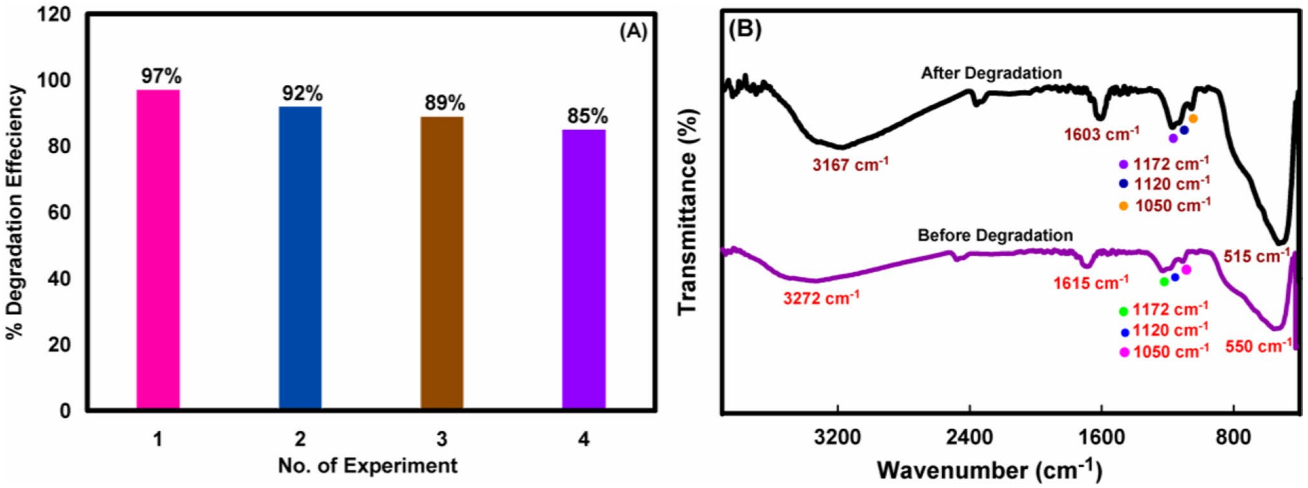

Fig. 10 (**A**) Reusability of the proposed photocatalyst for consecutive four times and (**B**) FTIR spectra of the proposed catalyst before and after CY degradation. Catalyst dosage: 5 g L^{-1}, [CY] = 5 mgL^{-1}, pH ~ 7.0, temp. = 25 °C

Table 2 Comparison of different TiO_2 photocatalyst against the proposed photocatalyst

Catalyst	Pollutant	Light source	Time	Degradation efficiency	Ref
Cu_x/TiO_2	RG 12	LEDs	360 min	53.4%	Zeghioud et al. (2019)
Ce-TiO_2	Glyphosate	Hg Lamp	60 min	76%	Xue et al. (2011)
BiOCl/TiO_2	MO	Sunlight	220 min	39%	Li et al. (2014)
B-Y-TiO_2	Phenol	UV–Vis DRS	240 min	89%	Shi et al. (2010)
P-doped TiO_2/MWCNTs	MB	Sunlight	240 min	55%	Sarker et al. (2022)
$TiO_{2-x}N_x$	MB	Visible light	180 min	91%	Asahi et al. (2001)
$CeTiO_2$/Eu-TiO_2	AB	UV–Vis	180 min	99.6%	Hamdi et al. (2021b)
Pt–TiO_2/zeolites	MO	UV–Vis	30 min	86.2%	Huang et al. (2008)
TiO_2-5 wt% (Ce-Bi-N)	CY	Sunlight	120 min	97.18%	**This work**

RG 12 reactive green 12, *MO* methyl orange, *MB* methylene blue, *CY* chlorazol yellow

adsorption–desorption equilibrium 30 min before photolysis, the catalyst was able to totally breakdown the CY dye after 120 min of photolysis. The adsorption of CY on the catalyst was driven by pseudo-second-order kinetics here. As determined by the degradation kinetics, the CY degradation follows a first order below 23.5 mg L^{-1}. However, beyond this concentration, the reaction order becomes fractional. Furthermore, a free energy of – 25.5 kJ mol^{-1} was estimated, implying pure spontaneous degradation of CY dye. Moreover, scavenging effect renders that superoxide and hydroxyl radicals have essential influence on the proposed degradation mechanism. From the evaluation of the stability and the reusability, this can be proposed as a competent photocatalyst for CY dye degradation which also could also be an efficient anti-tonic for cationic dye and other industrial effluents, or wastewater compared to different TiO_2 oxide-based photocatalyst. Moreover, in this work, the influence of pH was not mentioned due to the inconsistency of catalytic performance found in acidic conditions. On further hypothesis, boron-doped TiO_2 with the optimization of other competent dopants is supposed to be more efficient, which is the focus of our future research.

Supplementary Information The online version contains supplementary material available at https://doi.org/10.1007/s11356-022-24220-0.

Author contribution Zannatul Mumtarin Moushumy: writing original draft, investigation, Mohammad Jobaer Hassan: data curation, investigation, formal analysis, Mohebul Ahsan: investigation, visualization, validation, Md. Mahmudul Hasan: characterization, Md Nizam Uddin: conceptualization, Yuki Nagao: characterization, Mohammad A. Hasnat: investigation, validation, formal analysis, writing—review and editing.

Funding The authors received financial supports from the Ministry of Education, Bangladesh (Grant No. PS 20201512) and Shahjalal University of Science and Technology (PS/2022/1/01) to Mohammad A. Hasnat. Yuki Nagao appreciated the support by JSPS KAKENHI (JP21H00020) and JST CREST (JPMJCR21B3), Japan.

Data availability The authors declare that all data and materials as well as software application or custom code support their published claims and comply with field standards.

Declarations

Competing interests The authors declare no competing interests.

Disclaimer The result presented here is honest and clear without data manipulation.

References

Abdullah EA, Abdullah AH, Zainal Z et al (2012) Synthesis and characterisation of Penta-bismuth Hepta-oxide nitrate, $Bi_5O_7NO_3$, as a new adsorbent for methyl orange removal from an aqueous solution. E-Journal Chem 9:2429–2438. https://doi.org/10.1155/2012/707853

Agrawal K, Bhatt A, Bhardwaj N et al (2020) Integrated approach for the treatment of industrial effluent by physico-chemical and microbiological process for sustainable environment. Combined Application of Physico-Chemical & Microbiological Processes for Industrial Effluent Treatment Plant. Springer, Singapore, pp 119–143

Akrami A, Niazi A (2016) Synthesis of maghemite nanoparticles and its application for removal of Titan yellow from aqueous solutions using full factorial design. Desalin Water Treat 57:22618–22631. https://doi.org/10.1080/19443994.2015.1136693

Akter N, Hossain MA, Hassan MJ et al (2016) Amine modified tannin gel for adsorptive removal of Brilliant Green dye. J Environ Chem Eng 4:1231–1241. https://doi.org/10.1016/j.jece.2016.01.013

Alansi AM, Al-Qunaibit M, Alade IO et al (2018) Visible-light responsive BiOBr nanoparticles loaded on reduced graphene oxide for photocatalytic degradation of dye. J Mol Liq 253:297–304. https://doi.org/10.1016/j.molliq.2018.01.034

Alderete BL, da Silva J, Godoi R et al (2021) Evaluation of toxicity and mutagenicity of a synthetic effluent containing azo dye after advanced oxidation process treatment. Chemosphere 263:128291. https://doi.org/10.1016/j.chemosphere.2020.128291

Ali H, Guler AC, Masar M et al (2021) Solid-state synthesis of direct z-scheme Cu_2O/WO_3 nanocomposites with enhanced visible-light photocatalytic performance. Catalysts 11:1–26. https://doi.org/10.3390/catal11020293

Ani IJ, Akpan UG, Olutoye MA, Hameed BH (2018) Photocatalytic degradation of pollutants in petroleum refinery wastewater by TiO_2- and ZnO-based photocatalysts: recent development. J Clean Prod 205:930–954

Ansari SA, Khan MM, Ansari MO, Cho MH (2016) Nitrogen-doped titanium dioxide (N-doped TiO_2) for visible light photocatalysis. New J Chem 40:3000–3009

Arifin MN, Tarek M, Rahman Khan MM (2022) Efficient treatment of organic pollutants by boron doped TiO_2 photocatalysts under visible light radiation. Chem Eng Res Des 180:212–219. https://doi.org/10.1016/j.cherd.2022.02.016

Asahi R, Morikawa T, Ohwaki T et al (2001) Visible-light photocatalysis in nitrogen-doped titanium oxides. Science (80-) 293:269–271. https://doi.org/10.1126/science.1061051

Asl SK, Sadrnezhaad SK, Rad MK, Üner D (2012) Comparative photodecolorization of red dye by anatase, rutile (TiO_2), and wurtzite (ZnO) using response surface methodology. Turkish J Chem 36:121–135. https://doi.org/10.3906/kim-1104-31

Astuti Y, Listyani BM, Suyati L, Darmawan A (2021) Bismuth oxide prepared by sol-gel method: variation of physicochemical characteristics and photocatalytic activity due to difference in calcination temperature. Indones J Chem 21:108–117. https://doi.org/10.22146/ijc.53144

Bazin I, Ibn Hadj Hassine A, Haj Hamouda Y et al (2012) Estrogenic and anti-estrogenic activity of 23 commercial textile dyes. Ecotoxicol Environ Saf 85:131–136. https://doi.org/10.1016/j.ecoenv.2012.08.003

Benkhaya S, M'rabet S, El Harfi A (2020) Classifications, properties, recent synthesis and applications of azo dyes. Heliyon 6:e03271

Bharti B, Kumar S, Lee HN, Kumar R (2016) Formation of oxygen vacancies and Ti^{3+} state in TiO_2 thin film and enhanced optical properties by air plasma treatment. Sci Rep 6. https://doi.org/10.1038/srep32355

Bilgin Simsek E (2017) Solvothermal synthesized boron doped TiO_2 catalysts: photocatalytic degradation of endocrine disrupting compounds and pharmaceuticals under visible light irradiation. Appl Catal B Environ 200:309–322. https://doi.org/10.1016/j.apcatb.2016.07.016

Breault TM, Bartlett BM (2012) Lowering the band gap of anatase-structured TiO_2 by coalloying with Nb and N: Electronic structure and photocatalytic degradation of methylene blue dye. J Phys Chem C 116:5986–5994. https://doi.org/10.1021/jp2078456

Caner N, Kiran I, Ilhan S, Iscen CF (2009) Isotherm and kinetic studies of Burazol Blue ED dye biosorption by dried anaerobic sludge. J Hazard Mater 165:279–284. https://doi.org/10.1016/j.jhazmat.2008.09.108

Chen L, Guo W, Yang Y et al (2013) Morphology-controlled preparation and enhanced simulated sunlight and visible-light photocatalytic activity of Pt/$Bi_5Nb_3O_{15}$ heterostructures. Phys Chem Chem Phys 15:8342–8351. https://doi.org/10.1039/c3cp00084b

Chu L, Duo F, Zhang M et al (2020) Doping induced enhanced photocatalytic performance of SnO_2:Bi^{3+} quantum dots toward organic pollutants. Colloids Surfaces A Physicochem Eng Asp 589:124416. https://doi.org/10.1016/j.colsurfa.2020.124416

Çiçek F, Özer D, Özer A, Özer A (2007) Low cost removal of reactive dyes using wheat bran. J Hazard Mater 146:408–416. https://doi.org/10.1016/j.jhazmat.2006.12.037

Cravanzola S, Cesano F, Gaziano F, Scarano D (2017) Sulfur-doped TiO_2: structure and surface properties. Catalysts 7:214. https://doi.org/10.3390/catal7070214

Danmaliki GI, Saleh TA (2017) Effects of bimetallic Ce/Fe nanoparticles on the desulfurization of thiophenes using activated carbon. Chem Eng J 307:914–927. https://doi.org/10.1016/j.cej.2016.08.143

DeVito SC (1993) Predicting azo dye toxicity. Crit Rev Environ Sci Technol 23:249–324. https://doi.org/10.1080/10643389309388453

Ferreira FV, Souza LP, Martins TMM et al (2019) Nanocellulose/bioactive glass cryogels as scaffolds for bone regeneration. Nanoscale 11:19842–19849. https://doi.org/10.1039/c9nr05383b

Fried R, Oprea I, Fleck K, Rudroff F (2022) Biogenic colourants in the textile industry – a promising and sustainable alternative to synthetic dyes. Green Chem 24:13–35

Gičević A, Hindija L, Karačić A (2020) Toxicity of azo dyes in pharmaceutical industry. IFMBE Proceedings. Springer, Cham, pp 581–587

GilPavas E, Dobrosz-Gómez I, Gómez-García MÁ (2020) Efficient treatment for textile wastewater through sequential electrocoagulation, electrochemical oxidation and adsorption processes: optimization and toxicity assessment. J Electroanal Chem 878:114578. https://doi.org/10.1016/j.jelechem.2020.114578

Gürses A, Açıkyıldız M, Güneş K, Gürses MS (2016) Classification of dye and pigments. Springer, Cham, pp 31–45

Hamdi D, Mansouri L, Srivastava V et al (2021) Enhancement of Eu and Ce doped TiO_2 thin films photoactivity: application on amido black photodegradation. Inorg Chem Commun 133:108912. https://doi.org/10.1016/j.inoche.2021.108912

Hasani K, Moradi M, Mokhtari SA et al (2021) Degradation of basic violet 16 dye by electro-activated persulfate process from aqueous solutions and toxicity assessment using microorganisms: determination of by-products, reaction kinetic and optimization using Box-Behnken design. Int J Chem React Eng 19:261–275. https://doi.org/10.1515/ijcre-2020-0226

Hasnat MA, Uddin MM, Samed AJF et al (2007) Adsorption and photocatalytic decolorization of a synthetic dye erythrosine on anatase TiO_2 and ZnO surfaces. J Hazard Mater 147:471–477. https://doi.org/10.1016/j.jhazmat.2007.01.040

Hassani A, Eghbali P (2018) Metin Ö (2018) Sonocatalytic removal of methylene blue from water solution by cobalt ferrite/mesoporous graphitic carbon nitride ($CoFe_2O_4$/mpg-C_3N_4) nanocomposites: response surface methodology approach. Environ Sci Pollut Res 2532(25):32140–32155. https://doi.org/10.1007/S11356-018-3151-3

Hassani A, Faraji M, Eghbali P (2020) Facile fabrication of mpg-C_3N_4/Ag/ZnO nanowires/Zn photocatalyst plates for photodegradation of dye pollutant. J Photochem Photobiol A Chem 400:112665. https://doi.org/10.1016/J.JPHOTOCHEM.2020.112665

Helmy ET, Nemr AE, Mousa M, Arafa E, Eldafrawy S (2018) Photocatalytic degradation of organic dyes pollutants in the industrial textile wastewater by using synthesized TiO_2, C-doped TiO_2, S-doped TiO_2 and C,S co-doped TiO_2 nanoparticles. J Water Environ Nanotechnol 3:116–127. https://doi.org/10.22090/jwent.2018.02.003

Hemalatha P, Karthick SN, Hemalatha KV et al (2016) La-doped ZnO nanoflower as photocatalyst for methylene blue dye degradation under UV irradiation. J Mater Sci Mater Electron 27:2367–2378. https://doi.org/10.1007/s10854-015-4034-8

Hiremath S, Antony Raj MAL, Chandra Prabha MN, Vidya C (2018) Tamarindus indica mediated biosynthesis of nano TiO_2 and its application in photocatalytic degradation of Titan yellow. J Environ Chem Eng 6:7338–7346. https://doi.org/10.1016/j.jece.2018.08.052

Hu Y, Li D, Zheng Y et al (2011) $BiVO_4$/TiO_2 nanocrystalline heterostructure: a wide spectrum responsive photocatalyst towards the highly efficient decomposition of gaseous benzene. Appl Catal B Environ 104:30–36. https://doi.org/10.1016/j.apcatb.2011.02.031

Huang M, Xu C, Wu Z et al (2008) Photocatalytic discolorization of methyl orange solution by Pt modified TiO_2 loaded on natural zeolite. Dye Pigment 77:327–334. https://doi.org/10.1016/J.DYEPIG.2007.01.026

Huang W, Cheng H, Feng J et al (2018) Synthesis of highly water-dispersible N-doped anatase titania based on low temperature solvent-thermal method. Arab J Chem 11:871–879. https://doi.org/10.1016/j.arabjc.2017.12.028

Hübner K (2006) 150 jahre mauvein. Chemie Unserer Zeit 40:274–275

Jamee R, Siddique R (2019) Biodegradation of synthetic dyes of textile effluent by microorganisms: an environmentally and economically sustainable approach. Eur J Microbiol Immunol 9:114–118. https://doi.org/10.1556/1886.2019.00018

Jang MH, Hwang YS (2018) Effects of functionalized multi-walled carbon nanotubes on toxicity and bioaccumulation of lead in Daphnia magna. PLoS One 13. https://doi.org/10.1371/journal.pone.0194935

Kalantary RR, Dadban Shahamat Y, Farzadkia M et al (2015) Photocatalytic degradation and mineralization of diazinon in aqueous solution using nano-TiO_2(Degussa, P25): kinetic and statistical analysis. Desalin Water Treat 55:555–563. https://doi.org/10.1080/19443994.2014.928795

Karim AV, Hassani A, Eghbali P, Nidheesh PV (2022) Nanostructured modified layered double hydroxides (LDHs)-based catalysts: a review on synthesis, characterization, and applications in water remediation by advanced oxidation processes. Curr Opin Solid State Mater Sci 26:100965. https://doi.org/10.1016/J.COSSMS.2021.100965

Khan MM, Ansari SA, Pradhan D et al (2014) Band gap engineered TiO_2 nanoparticles for visible light induced photoelectrochemical and photocatalytic studies. J Mater Chem A 2:637–644. https://doi.org/10.1039/c3ta14052k

Khan R, Bhawana P, Fulekar MH (2013) Microbial decolorization and degradation of synthetic dyes: a review. Rev Environ Sci Biotechnol 12:75–97

Kishor R, Purchase D, Saratale GD et al (2021) Ecotoxicological and health concerns of persistent coloring pollutants of textile industry wastewater and treatment approaches for environmental safety. J Environ Chem Eng 9:105012. https://doi.org/10.1016/j.jece.2020.105012

Kovalevskiy N, Selishchev D, Svintsitskiy D et al (2020) Synergistic effect of polychromatic radiation on visible light activity of N-doped TiO_2 photocatalyst. Catal Commun 134:105841. https://doi.org/10.1016/j.catcom.2019.105841

Li H, Liu J, Qian J et al (2014) Preparation of Bi-doped TiO_2 nanoparticles and their visible light photocatalytic performance. Cuihua Xuebao/chinese J Catal 35:1578–1589. https://doi.org/10.1016/S1872-2067(14)60124-8

Li Y, Yang Z, Wang Y et al (2017) A mesoporous cationic thorium-organic framework that rapidly traps anionic persistent organic pollutants. Nat Commun 8:1–11. https://doi.org/10.1038/s41467-017-01208-w

Liu G, Feng M, Tayyab M et al (2021) Direct and efficient reduction of perfluorooctanoic acid using bimetallic catalyst supported on carbon. J Hazard Mater 412:125224. https://doi.org/10.1016/J.JHAZMAT.2021.125224

Liu T, Wang L, Lu X et al (2017) Comparative study of the photocatalytic performance for the degradation of different dyes by $ZnIn_2S_4$: adsorption, active species, and pathways. RSC Adv 7:12292–12300. https://doi.org/10.1039/C7RA00199A

Liu Y, Yu H, Lv Z et al (2012) Simulated-sunlight-activated photocatalysis of Methylene Blue using cerium-doped SiO_2/TiO_2 nanostructured fibers. J Environ Sci (china) 24:1867–1875. https://doi.org/10.1016/S1001-0742(11)61008-5

Luo L, Sun L, Long Y et al (2019) Multiferroic properties of aurivillius structure $Bi_4SmFeTi_3O_{15}$ thin films. J Mater Sci Mater Electron 30:9945–9954. https://doi.org/10.1007/s10854-019-01334-9

Milosevic I, Jayaprakash A, Greenwood B et al (2017) Synergistic effect of fluorinated and N doped TiO_2 nanoparticles leading to different microstructure and enhanced photocatalytic bacterial inactivation. Nanomater 7:391. https://doi.org/10.3390/NANO7110391

Milošević I, Rtimi S, Jayaprakash A et al (2018) Synthesis and characterization of fluorinated anatase nanoparticles and subsequent N-doping for efficient visible light activated photocatalysis. Colloids Surfaces B Biointerfaces 171:445–450. https://doi.org/10.1016/j.colsurfb.2018.07.035

Mishra G, Mukhopadhyay M (2019) TiO_2 decorated functionalized halloysite nanotubes (TiO_2@HNTs) and photocatalytic PVC membranes synthesis, characterization and its application in water treatment. Sci Rep 9. https://doi.org/10.1038/s41598-019-40775-4

Modwi A, Ghanem MA, Al-Mayouf AM, Houas A (2018) Lowering energy band gap and enhancing photocatalytic properties of Cu/ZnO composite decorated by transition metals. J Mol Struct 1173:1–6. https://doi.org/10.1016/j.molstruc.2018.06.082

Murcia-López S, Hidalgo MC, Navío JA (2011) Synthesis, characterization and photocatalytic activity of Bi-doped TiO_2 photocatalysts under simulated solar irradiation. Appl Catal A Gen 404:59–67. https://doi.org/10.1016/j.apcata.2011.07.008

Nawaz MS, Ahsan M (2014) Comparison of physico-chemical, advanced oxidation and biological techniques for the textile wastewater treatment. Alexandria Eng J 53:717–722. https://doi.org/10.1016/j.aej.2014.06.007

Niu P, Wu G, Chen P et al (2020) Optimization of boron doped TiO_2 as an efficient visible light-driven photocatalyst for organic dye degradation with high reusability. Front Chem 8:172. https://doi.org/10.3389/fchem.2020.00172

Ozensoy E, Peden CHF, Szanyi J (2005) NO_2 adsorption on ultrathin θ-Al_2O_3 films: formation of nitrite and nitrate species. J Phys Chem B 109:15977–15984. https://doi.org/10.1021/jp052053e

Pan D, Chen J, Yao S et al (2005) An amperometric glucose biosensor based on glucose oxidase immobilized in electropolymerized poly(*o*-aminophenol) and carbon nanotubes composite film on a gold electrode. Anal Sci 21:367–371. https://doi.org/10.2116/analsci.21.367

Qi D, Xing M, Zhang J (2014) Hydrophobic carbon-doped TiO_2/MCF-F composite as a high performance photocatalyst. J Phys Chem C 118:7329–7336. https://doi.org/10.1021/jp4123979

Radoičić MB, Janković IA, Despotović VN et al (2013) The role of surface defect sites of titania nanoparticles in the photocatalysis: aging and modification. Appl Catal B Environ 138–139:122–127. https://doi.org/10.1016/j.apcatb.2013.02.032

Saadati F, Keramati N, Ghazi MM (2016) Influence of parameters on the photocatalytic degradation of tetracycline in wastewater: a review. Crit Rev Environ Sci Technol 46:757–782

Sakr F, Alahiane S, Sennaoui A et al (2020) Removal of cationic dye (Methylene Blue) from aqueous solution by adsorption on two type of biomaterial of South Morocco. Materialstoday: Proceedings 22:93–96.https://doi.org/10.1016/j.matpr.2019.08.101

Sarker DR, Uddin MN, Elias M et al (2022) P-doped TiO_2-MWCNTs nanocomposite thin films with enhanced photocatalytic activity under visible light exposure. Clean Eng Technol 6:100364. https://doi.org/10.1016/j.clet.2021.100364

Shi Z, Liu F, Yao S (2010) Preparation and photocatalytic activity of B, y co-doped nanosized TiO_2 catalyst. J Rare Earths 28:737–741. https://doi.org/10.1016/S1002-0721(09)60191-5

Sinha K, Chowdhury S, Das SP, Datta S (2013) Modeling of microwave-assisted extraction of natural dye from seeds of Bixa orellana (Annatto) using response surface methodology (RSM) and artificial neural network (ANN). Ind Crops Prod 41:165–171. https://doi.org/10.1016/j.indcrop.2012.04.004

Ben SH, Bouket AC, Pourhassan Z et al (2021) Diversity of synthetic dyes from textile industries, discharge impacts and treatment methods. Appl Sci 11:6255. https://doi.org/10.3390/app11146255

Tang WZ, An H (1995) UV/TiO_2 photocatalytic oxidation of commercial dyes in aqueous solutions. Chemosphere 31:4157–4170. https://doi.org/10.1016/0045-6535(95)80015-D

Tauc J, Grigorovici R, Vancu A (1966) Optical properties and electronic structure of amorphous germanium. Phys Status Solidi 15:627–637. https://doi.org/10.1002/pssb.19660150224

Teo SH, Ng CH, Islam A et al (2022) Sustainable toxic dyes removal with advanced materials for clean water production: a comprehensive review. J Clean Prod 332:130039

Uddin MM, Hasnat MA, Samed AJF, Majumdar RK (2007) Influence of TiO_2 and ZnO photocatalysts on adsorption and degradation behaviour of Erythrosine. Dye Pigment 75:207–212. https://doi.org/10.1016/j.dyepig.2006.04.023

Varnagiris S, Medvids A, Lelis M et al (2019) Black carbon-doped TiO_2 films: synthesis, characterization and photocatalysis. J Photochem Photobiol A Chem 382:111941. https://doi.org/10.1016/j.jphotochem.2019.111941

Vidya C, Manjunatha C, Sudeep M et al (2020) Photo-assisted mineralisation of titan yellow dye using ZnO nanorods synthesised via environmental benign route. SN Appl Sci 2:1–15. https://doi.org/10.1007/S42452-020-2537-2/FIGURES/11

Vidya C, Prabha MNC, Raj MALA (2016) Green mediated synthesis of zinc oxide nanoparticles for the photocatalytic degradation of Rose Bengal dye. Environ Nanotechnology, Monit Manag 6:134–138. https://doi.org/10.1016/j.enmm.2016.09.004

Wahi RK, Yu WW, Liu Y et al (2005) Photodegradation of Congo Red catalyzed by nanosized TiO_2. J Mol Catal A Chem 242:48–56. https://doi.org/10.1016/j.molcata.2005.07.034

Wang HY, Li B, Teng JX et al (2017) N-doped carbon-coated TiN exhibiting excellent electrochemical performance for supercapacitors. Electrochim Acta 257:56–63. https://doi.org/10.1016/j.electacta.2017.10.066

Wei X, Zhu G, Fang J, Chen J (2013) Synthesis, characterization, and photocatalysis of well-dispersible phase-pure anatase TiO_2 nanoparticles. Int J Photoenergy 2013. https://doi.org/10.1155/2013/726872

Worayingyong A, Sang-urai S, Smith MF et al (2014) Effects of cerium dopant concentration on structural properties and photocatalytic activity of electrospun Ce-doped TiO_2 nanofibers. Appl Phys A Mater Sci Process 117:1191–1201. https://doi.org/10.1007/s00339-014-8501-5

Xiong Z, Zhao Y, Zhang J, Zheng C (2015) Efficient photocatalytic reduction of CO_2 into liquid products over cerium doped titania nanoparticles synthesized by a sol-gel auto-ignited method. Fuel Process Technol 135:6–13. https://doi.org/10.1016/j.fuproc.2014.09.017

Xue W, Zhang G, Xu X et al (2011) Preparation of titania nanotubes doped with cerium and their photocatalytic activity for glyphosate. Chem Eng J 167:397–402. https://doi.org/10.1016/j.cej.2011.01.007

Yagub MT, Sen TK, Afroze S, Ang HM (2014) Dye and its removal from aqueous solution by adsorption: a review. Adv Colloid Interface Sci 209:172–184

Yan X, Yuan K, Lu N et al (2017) The interplay of sulfur doping and surface hydroxyl in band gap engineering: mesoporous sulfur-doped TiO_2 coupled with magnetite as a recyclable, efficient, visible light active photocatalyst for water purification. Appl Catal B Environ 218:20–31. https://doi.org/10.1016/j.apcatb.2017.06.022

Yaseen DA, Scholz M (2019) Textile dye wastewater characteristics and constituents of synthetic effluents: a critical review. Int J Environ Sci Technol 16:1193–1226

Yim S-D, Chung HT, Chlistunoff J et al (2015) A microelectrode study of interfacial reactions at the platinum-alkaline polymer interface. J Electrochem Soc 162:F499–F506. https://doi.org/10.1149/2.0151506jes

Yu L, Shao Y, Li D (2017) Direct combination of hydrogen evolution from water and methane conversion in a photocatalytic system over Pt/TiO_2. Appl Catal B Environ 204:216–223. https://doi.org/10.1016/j.apcatb.2016.11.039

Zeghioud H, Assadi AA, Khellaf N et al (2019) Photocatalytic performance of Cu_xO/TiO_2 deposited by HiPIMS on polyester under visible light LEDs: oxidants, ions effect, and reactive oxygen species investigation. Mater 12:412. https://doi.org/10.3390/MA12030412

Zhu SR, Wu MK, Zhao WN et al (2017) Fabrication of heterostructured $BiOBr/Bi_{24}O_{31}Br_{10}/TiO_2$ photocatalyst by pyrolysis of MOF composite for dye degradation. J Solid State Chem 255:17–26. https://doi.org/10.1016/j.jssc.2017.07.038

The authors can declare that the research is original and have not been published anywhere in any languages.

Authors and Affiliations

Zannatul Mumtarin Moushumy[1] · **Mohammad Jobaer Hassan**[1] · **Mohebul Ahsan**[1] · **Md. Mahmudul Hasan**[2] · **Md. Nizam Uddin**[1] · **Yuki Nagao**[2] · **Mohammad A. Hasnat**[1]

[1] Electrochemistry & Catalysis Research Laboratory (ECRL), Department of Chemistry, School of Physical Sciences, Shahjalal University of Science and Technology, Sylhet 3114, Bangladesh

[2] School of Materials Science, Japan Advanced Institute of Science and Technology, 1-1 Asahidai, Nomi, Ishikawa 923-1292, Japan